Narrow Subthreshold Quantum Mechanical Resonances in the Li + HF → H + LiF Reaction†

Liqiang Wei, Ahren W. Jasper, and Donald G. Truhlar*

Department of Chemistry and Supercomputing Institute, University of Minnesota, Minneapolis, Minnesota 55455-0431

Received: February 28, 2003; In Final Form: April 30, 2003

State-to-state, state-specific, and cumulative reaction probabilities are presented for the bimolecular scattering process Li + HF → H + LiF in the ground electronic state. Calculations were performed for zero total angular momentum at total energies from 0.26 to 0.50 eV (relative to HF at its classical equilibrium bond distance and infinitely far from Li). The energy dependence of the state-to-state, initial-state-selected, and cumulative reaction probabilities for LiFH in the low-energy regime displays a pronounced resonance structure due to quasibound states associated with a Li···FH van der Waals well in the entrance valley of the potential energy surface. The lifetimes of the long-lived resonances are obtained by fitting the calculated eigenphase sum to the multichannel Breit−Wigner formula. The final rotational state distributions of the LiF product fragment resulting from decay of the resonance state complexes are presented for two resonances. Quantum numbers are assigned to the resonances using bound-state and quasibound-state calculations in the Li···FH van der Waals well, and possible decay mechanisms are discussed. The lifetimes show a systematic dependence on the translational vibrational quantum number.

1. Introduction

The reaction Li + HF → H + LiF has become a prototype for both theoretical and experimental investigations of the dynamics of atom−diatom systems with three different atoms and the heavy−heavy−light mass combination. The ground-state potential energy surface has been calculated, and several analytic fits have been presented in the literature.[1−17] Various aspects of the dynamics of LiFH have been studied, including reactive collisions,[10,11,18−32] stereodynamics and vector correlations,[26,29,30,33−35] and photodissociation dynamics.[15,36−39] Experimentally observable quantities such as the differential and integral cross sections have also been discussed.[18,20,26,29,30]

A striking feature of the previously reported studies is the strong resonance structure.[10,11,19,21−25,28,32] It is well-known that resonance structure in dynamical features may be associated with quasibound (i.e., metastable) states of the system. However, in all of the investigations carried out so far for the Li + HF reaction, the description of the resonance structure is phenomenological, and there is little quantitative characterization. In addition, research has been primarily focused on the scattering features, and there is no study of the intermediate metastable states of the Li···FH complexes, which are of fundamental interest. One objective in the present study is to identify the energies and lifetimes of the resonance states using fully converged quantum mechanical scattering calculations. The method employed is a time-independent, two-arrangement Green's-function-based scattering approach, namely the outgoing scattering wave variational principle (OWVP).[40−43] The results are limited by the accuracy of the fitted multidimensional potential energy surface.

The present work is especially timely in light of the recent work of Bowman, Manolopoulos, and co-workers,[44,45] in which subthreshold resonances associated with the van der Waals wells of the HOCl system were identified in exact quantum mechanical scattering calculations and characterized using quasibound-state calculations. A similar analysis for the FH_2 system and its deuterated isotopes has demonstrated the existence of van der Waals well resonances.[46−48] In the present paper, we interpret observed resonances in the Li + HF reaction as due to metastable van der Waals complexes of the reactants, i.e., Li···FH van der Waals complexes.

This paper is organized as follows. Section 2 reviews the basic features of the ground-state potential energy surface for the reactive LiFH system. Section 3 contains a brief summary of the theory and methods that are used in the scattering and the bound- and quasibound-state calculations. In section 4, we present state-to-state, initial-state-selected, and cumulative reaction probabilities for total angular momentum $J = 0$. The resonance energies and widths are obtained by fitting the energy dependence of the eigenphase sum to the multichannel Breit−Wigner formula. The product rotational state distributions resulting from the decay of two resonances are also presented. The resonance complexes are further characterized by assigning vibrational quantum numbers corresponding to quasibound states of the Li···FH van der Waals complex. Section 5 is a summary.

2. Ground-State Potential Energy Surface of the LiFH Complex

Details of the ground-state LiFH potential energy surface used here have been presented previously.[15] Briefly, potential energies for the two lowest energy electronic surfaces were calculated at a high level of theory over a wide range of nuclear geometries. These adiabatic energies were fitted to analytic functional forms in the diabatic representation. The ground-state adiabatic potential energy surface used in the present study is obtained by diagonalizing the fitted diabatic potential energy matrix. The surface fit used here has been labeled surface fit **H** in later work.[16]

† Part of the special issue "Donald J. Kouri Festschrift".

10.1021/jp0345250 CCC: $25.00
Published on Web 06/12/2003

TABLE 1: Geometries and Energies of the Stationary Points for the Ground-State Potential Energy Surface of the Li + HF → H + LiF Reaction[a]

	geometry				energy[b]		
stationary point	R_{HF}[c]	R_{LiF}	R_{LiH}	θ_{LiFH}[d]	V	ZPE	V + ZPE
reactant (A)[e]	1.733				0.000	0.255	0.255
reactant well (B)	1.750	3.563	4.483	110	−0.211	0.281	0.070
first saddle point (C)	2.422	3.151	3.379	73.3	0.352	0.098	0.451
product well (D)	3.316	2.997	3.592	69.2	0.171	0.136	0.306
second saddle point (E)	4.506	2.957	5.294	87.8	0.227	0.062	0.290
product (F)		2.953			0.213	0.056	0.270

[a] Distances are in bohrs, angles are in degrees, and energies are in electron volts. [b] The zero-point energies (ZPE) were calculated using the Morse I approximation[46,47] with the *POLYRATE* software package.[48] [c] R_{AB} is the internuclear distance between atoms A and B. [d] θ_{LiFH} is the Li−F−H bond angle. [e] The letters A−F correspond to the features labeled in Figure 1.

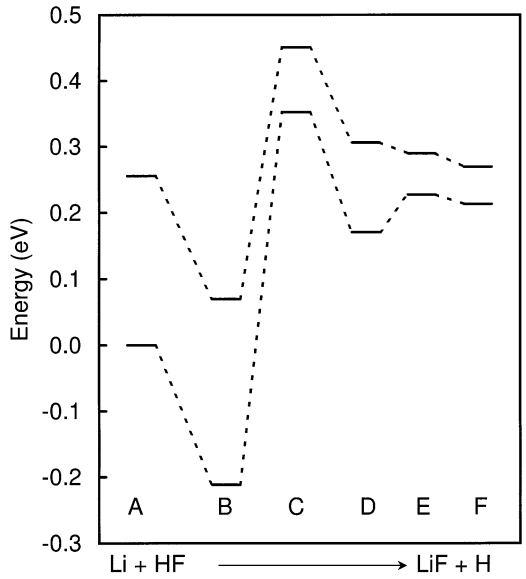

Figure 1. Relative energies of stationary points of Li + HF → H + LiF reaction on the electronic ground-state potential energy surface. The features labeled A−F are described in Table 1 and correspond to (A) reactants, (B) the reactant van der Waals well, i.e., Li···FH, (C) the saddle point, (D) the product van der Waals well, i.e., LiF···H, (E) the product saddle point, and (F) products. The lower potential scheme is zero-point exclusive, and the upper potential scheme is zero-point inclusive. The zero-point energy that is included is from one mode at A and F, from two modes at C and E, and from three modes at B and D.

The ground-state surface has two van der Waals wells: one in the entrance valley with a well depth of 0.21 eV with respect to the Li + HF asymptote at its equilibrium geometry, and the other in the product valley with a well depth of 0.043 eV with respect to the LiF + H asymptote at its equilibrium geometry. The surface also has two saddle points. The first saddle point is the transition state for the F transfer reaction and has a nonlinear geometry and a potential barrier height of 0.35 eV with respect to the Li + HF asymptote at its equilibrium geometry. The second saddle point is the transition state for dissociation of the LiF···H complex and has a very small height of 0.014 eV with respect to the LiF + F asymptote at its equilibrium geometry and is located in the product valley. The overall reaction Li + HF → LiF + H is endoergic by 0.21 eV without including the zero-point energy of the reactants and products and by 0.015 eV when zero-point energy is included. The characteristic features of the stationary points of the ground-state LiFH surface are summarized in Table 1 and are shown schematically in Figure 1. The zero-point energies in Table 1 are taken from ref 15 and were calculated using the Morse-I approximation[49,50] available in the POLYRATE[51] software package.

3. Theory

3.1. Quantum Mechanical Scattering Matrices. Quantum mechanical scattering matrix elements were obtained by solving the time-independent Schrödinger equation by the outgoing wave variational principle (OWVP).[40−43] In this method, the Schrödinger equation is solved by expanding the outgoing scattering waves in terms of internal-state channel functions for each asymptotic chemical arrangement. The solution to the Schrödinger equation can be written in integral form using the Lippmann−Schwinger formalism.[42,43,52,53] The first term in the solution is called the distorted wave and satisfies

$$(H_D^k - E)\Phi_{n_0}^{(+)k} = 0 \tag{1}$$

where H_D^k contains some of the channel-channel coupling, E is the total energy, k labels a chemical arrangement ($k = 1$ for the Li + HF arrangement and $k = 2$ for the H + LiF arrangement), n is the collection of quantum numbers describing the asymptotic state of the system (including the rotational, vibrational, and electronic states, and the chemical arrangement) and may be called an asymptotic channel, n_0 is the initial asymptotic channel, and $\Phi_{n_0}^{(+)k}$ is obtained by solving eq 1 numerically using finite differences.[41,54] The difference between the full Hamiltonian for arrangement k and the distorted wave Hamiltonian H_D^k is the coupling potential V_C^k. The contribution to the scattering matrix from V_C^k is obtained variationally using a dynamically adapted basis set.[40−43]

Using this two-step scheme, the full scattering matrix is written as the sum of two terms:

$$S_{nn_0} = \delta_{kk_0} S_{nn_0}^{0k} + \mathcal{S}_{nn_0} \tag{2}$$

where the first term is the distorted wave Born approximation for the scattering matrix obtained using the distorted wave functions $\Phi_{n_0}^{(+)k}$, and the second term is the contribution from the coupling potential V_C^k. Two kinds of basis functions are employed in the present study: half-integrated Green's functions[54] (called type-*g* basis functions) and asymptotic eigenstate basis functions (called type-*e* basis functions). The type-*g* basis functions are used for energetically open channels, and type-*e* basis functions are used for energetically closed channels. See refs 40−43 for more details regarding our implementation of the OWVP scattering algorithm.

After the scattering matrix is calculated, the transition probabilities and cumulative reaction probabilities may be obtained according to their usual definitions.

3.2. Resonance Scattering. A resonance may be characterized in terms of its resonance energy E_α and total width Γ_α, where the index α labels the resonance. These observables may be correlated with the analytic properties of the scattering matrix

such that the complex energies

$$z_\alpha = E_\alpha - \frac{i}{2}\Gamma_\alpha \tag{3}$$

are the poles of the scattering matrix elements.[52,55]

In the neighborhood of an isolated narrow resonance (INR), the scattering matrix elements $S_{nn'}(E)$ can be separated into background (nonresonant) contributions $S^b_{nn'}(E)$ and contributions from the resonance. This yields[52,55]

$$S_{nn'}(E) = S^b_{nn'}(E) - i\frac{\gamma_{\alpha n}\gamma_{\alpha n'}}{E - z_\alpha} \tag{4}$$

where $\gamma_{\alpha n}$ is the partial width amplitude for channel n and is related to the partial width by

$$\Gamma_{\alpha n} = |\gamma_{\alpha n}|^2 \tag{5}$$

Each partial width is related to the lifetime $\tau_{\alpha n}$ for the unimolecular decay of resonance state α into a specific final channel n:

$$\tau_{\alpha n} = \hbar/\Gamma_{\alpha n} \tag{6}$$

The sum over all of the partial widths for a given resonance α gives the total width of that resonance:

$$\Gamma_\alpha = \sum_n \Gamma_{\alpha n} \tag{7}$$

and the total width is related to the lifetime of the resonance:

$$\tau_\alpha = \hbar/\Gamma_\alpha \tag{8}$$

Using eqs 3 and 4 and ignoring the background contribution, one can obtain the state-to-state or channel-to-channel transition probability in the neighborhood of resonance

$$|S_{nn'}(E)|^2 = \frac{{\Gamma_\alpha}^2}{(E - E_\alpha)^2 + {\Gamma_\alpha}^2/4} P_{\alpha n} P_{\alpha n'} \tag{9}$$

where

$$P_{\alpha n} = \Gamma_{\alpha n}/\Gamma_\alpha \tag{10}$$

is the branching ratio, i.e., the probability for entering the resonance state α from the initial channel n (or equivalently the probability of leaving the resonance state α into the final channel n).

To extract the resonance energy and resonance width, it is convenient to use the expression for the eigenphase sum $\Delta(E)$, which is defined by

$$\exp[2i\Delta(E)] = \det[\mathbf{S}(E)] \tag{11}$$

As the total energy E passes close to a resonance energy z_n, the eigenphase sum increases rapidly by approximately π. This behavior can be expressed analytically using the multichannel Breit−Wigner formula,[56−58]

$$\Delta(E) = \Delta^b(E) + \arctan\left[\frac{\Gamma_\alpha}{2(E_\alpha - E)}\right] + m(E)\pi, \quad m = ..., -2, -1, 0, 1, 2, ... \tag{12}$$

where $\Delta^b(E)$ is the nonresonant or background contribution. The term $m(E)\pi$ indicates that eq 12 determines $\Delta(E)$ only within a factor of π, and for each value of E some integral multiple of π must be added to the eigenphase sum such that the eigenphase sum is a continuous function of E. The observables E_α and Γ_α may be extracted from $\Delta(E)$, by fitting the multichannel Breit−Wigner formula, eq 12, to the eigenphase sum data obtained from scattering calculations.[59−61]

Not all resonances are isolated and narrow. Overlapping resonances may occur and these resonance features involve strong interference effects and statistical behavior in contrast to the mode-specific behavior of the INRs.[62] The theoretical analysis of overlapping and broad resonances is much more complicated than the case of INRs and will not be considered here.

TABLE 2: Basis Set Parameters and Numerical Parameters for the Outgoing Scattering Wave Calculation for the Total Energy 0.4 eV[a]

basis set parameters	set 1	set 2	basis set parameters	set 1	set 2
j_{max} ($k=1,v=0$)	26	28	j_{max} ($k=2,v=3$)	56	62
j_{max} ($k=1,v=1$)	22	24	j_{max} ($k=2,v=4$)	50	56
j_{max} ($k=1,v=2$)	17	19	j_{max} ($k=2,v=5$)	43	50
j_{max} ($k=1,v=3$)	10	12	j_{max} ($k=2,v=6$)	35	43
j_{max} ($k=1,v=4$)		4	j_{max} ($k=2,v=7$)	24	35
N(HO) ($k=1$)	80	80	j_{max} ($k=2,v=8$)	14	24
m^g ($k=1$)	37	39	j_{max} ($k=2,v=9$)		2
m^e ($k=1$)	37	39	N(HO) ($k=2$)	80	80
$S_l{}^G(k=1)$	1.80	1.50	m^g ($k=2$)	35	37
$S_u{}^G(k=1)$	7.20	7.58	m^e ($k=2$)	35	37
Δ^S ($k=1$)	0.15	0.16	$S_l{}^G(k=2)$	1.80	1.50
w^S ($k=1$)	0.75	0.80	$S_u{}^G(k=2)$	6.56	6.90
j_{max} ($k=2,v=0$)	72	76	Δ^S ($k=2$)	0.14	0.15
j_{max} ($k=2,v=1$)	67	72	w^S ($k=2$)	0.75	0.80
j_{max} ($k=2,v=2$)	62	67			

numerical parameters	set 1	set 2	numerical parameters	set 1	set 2
N^{QV} ($k=1$)	20	25	ϵ_{rad}	7	9
N^{QA} ($k=1$)	75	80	ϵ_B	10	12
$N_e{}^{QA}(k=1)$	0	0	ϵ_W	10	12
$S_l{}^{QR}(k=1)$	1.5	1.3	$S_0{}^F(k=1)$	1.0	0.8
$S_u{}^{QR}(k=1)$	15	17	$S_{N(F)+1}{}^{QV}(k=1)$	20	22
N^{QGL} ($k=1$)	100	100	N^{FD} ($k=1$)	13	13
N^{QS} ($k=1$)	7	7	$N(F)$ ($k=1$)	730	733
N^{QV} ($k=2$)	20	25	N^{SD} ($k=1$)	30	33
N^{QA} ($k=2$)	75	80	f^{SD} ($k=1$)	0.9	0.9
$N_e{}^{QA}(k=2)$	75	80	$S_0{}^F(k=2)$	1.0	0.8
$S_l{}^{QR}(k=2)$	1.0	0.8	$S_{N(F)+1}{}^{QV}(k=2)$	25	27
$S_u{}^{QR}(k=2)$	15	17	N^{FD} ($k=2$)	11	11
N^{QGL} ($k=2$)	120	120	$N(F)$ ($k=2$)	870	873
N^{QS} ($k=2$)	7	7	N^{SD} ($k=2$)	30	33
e_c	10	12	f^{SD} ($k=2$)	0.9	0.9
ϵ_t	50	55			

[a] Atomic units are used.

3.3. Bound and Quasibound States of the Reactant van der Waals Well. The bound-state and quasibound-state energies and wave functions of the Li···FH van der Waals well were computed using the computer code ABCSPECTRA.[63] The bound-state and quasibound-state wave functions were expanded in the basis Γ_β

$$\Psi_\alpha(\mathbf{R},\mathbf{r}) = \sum_\beta c_{\alpha\beta}\Gamma_\beta(\mathbf{R},\mathbf{r}) \tag{13}$$

where

$$\Gamma_\beta(\mathbf{R},\mathbf{r}) = \frac{1}{R}t_m(R)\frac{1}{r}\phi_{vj}(r)\,y_{jl}(\hat{\mathbf{R}},\hat{\mathbf{r}}) \tag{14}$$

$\mathbf{R} = R\hat{\mathbf{R}}$ is the mass-scaled translational Jacobi coordinate

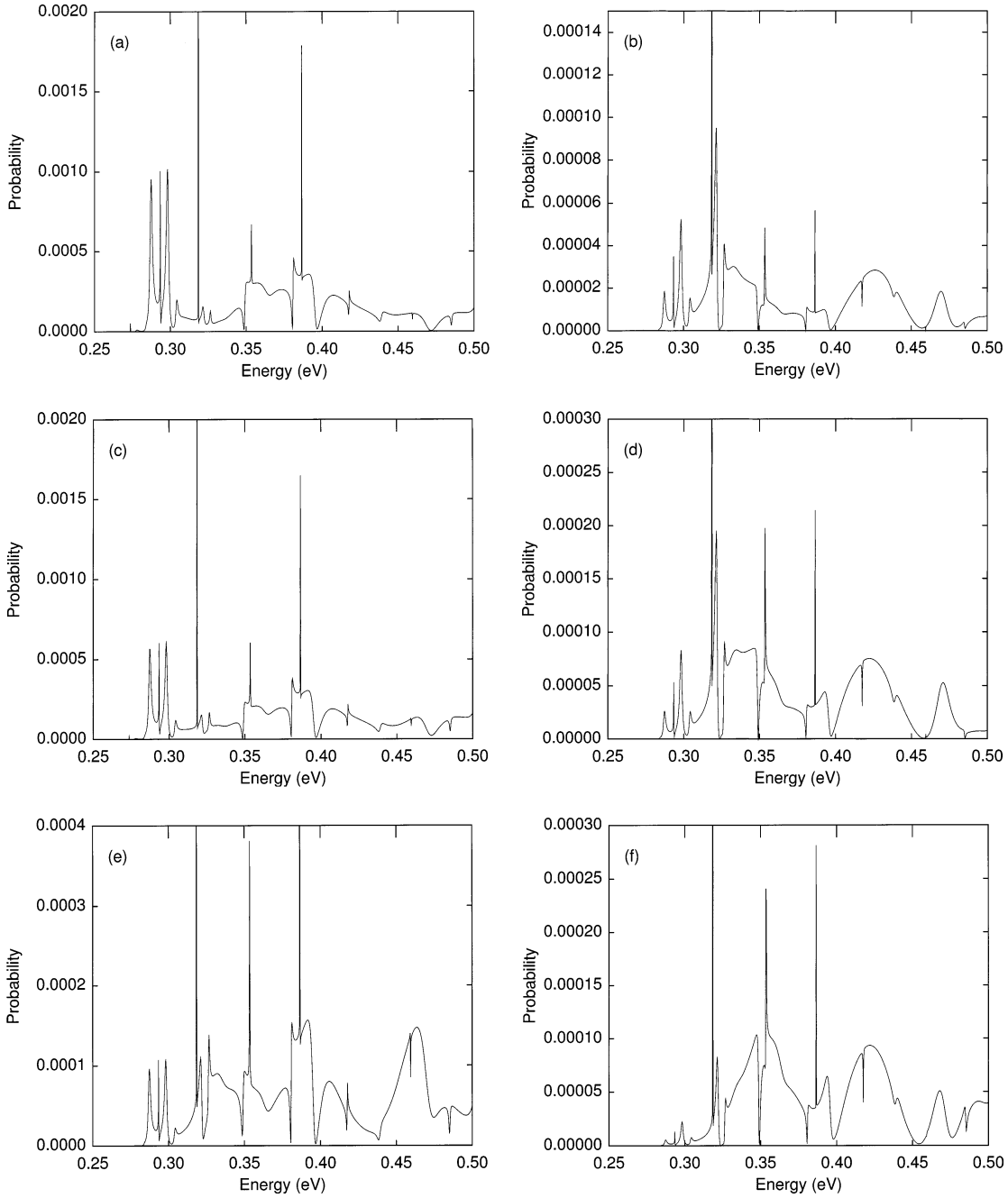

Figure 2. State-to-state reaction probabilities as a function of the total energy for the reaction Li + HF($v = 0$, $j = 0$) → H + LiF($v' = 0$, j'): (a) $j' = 0$, (b) $j' = 1$, (c) $j' = 2$, (d) $j' = 3$, (e) $j' = 4$, and (f) $j' = 5$.

describing the Li to center-of-mass of HF motion, $\mathbf{r} = r\hat{\mathbf{r}}$ is the mass-scaled internal Jacobi coordinate describing the HF vibrational motion, α is a collection of quantum numbers and labels the bound or quasibound state, $c_{\alpha\beta}$ is an expansion coefficient, t_m is a Gaussian translational basis function, ϕ_{vj} is an asymptotic eigenstate rovibrational function of HF, and y_{jl} is an eigenfunction of the total angular momentum $J = 0$, the rotational state of HF j, and the orbital angular momentum of Li with respect to the center of mass of HF l. The basis function index β is the collection of the indices v, j, l, and m, where v is the vibrational quantum number of the isolated diatom, and m labels the translational basis functions.

The expansion coefficients in eq 13 may be obtained by numerically computing the matrix elements

$$H_{\beta'\beta} = \langle\beta' H|\beta\rangle \equiv \int \Gamma_{\beta'} H \Gamma_{\beta}\, \mathrm{d}\mathbf{R}\, \mathrm{d}\mathbf{r} \tag{15}$$

$$S_{\beta'\beta} = \langle\beta'|\beta\rangle \equiv \int \Gamma_{\beta'} \Gamma_{\beta}\, \mathrm{d}\mathbf{R}\, \mathrm{d}\mathbf{r} \tag{16}$$

where H is the full Hamiltonian and solving the generalized eigenvalue problem. Details of the bound-state calculations including the computational implementation and the numerical and basis set parameters are given in the Appendix.

4. Results and Discussion

4.1. State-to-State, State-Selected, and Cumulative Reaction Probabilities. OWVP reactive scattering calculations were carried out at total energies ranging from 0.26 to 0.50 eV relative to the Li + HF asymptote at its equilibrium geometry using

version 18.8 of the VP scattering code.[64] To resolve the resonance states, we used an energy grid of 0.0001 eV at low energies. Resonance widths usually increase with energy, and therefore we used a coarser grid of 0.000 25 eV at high energies. Table 2 lists two sets of basis set and numerical parameters used for the scattering calculations at a total energy of 0.4 eV. The definitions of the parameters are given elsewhere.[42,43] At this energy, parameter set 1, for example, has a total of 511 asymptotic channels, of which 47 are open, and a total of 18 043 basis functions. The larger parameter set, parameter set 2, was used to check the convergence of the results with respect to variations in both the numerical and basis parameters. The state-to-state transition probabilities and eigenphase sums computed with parameter sets 1 and 2 differ from each other by no more than 1%.

Figure 2 shows the state-to-state reaction probability plotted as a function of energy for the process Li + HF($v = 0, j = 0$) → H + LiF($v' = 0, j'$), where $j' = 0-5$. A strong resonance structure dominates the energy profiles, especially in the energy region associated with the Li···FH van der Waals well in Figure 1. We note that, even at resonance energies, the probability of reaction is small (less than 0.1), and therefore nonreactive collisions are the dominant process. This is not surprising due to the 0.35 eV barrier and 0.23 eV endoergicity of the reaction, as shown in Figure 1.

Figure 3 presents the initial-state-selected reaction probability for the process Li + HF($v = 0, j$) → H + LiF, where $j = 0-9$. We see that the major resonances displayed in the state-to-state reaction probabilities persist after summing over final states. Note the strong dependence of the state-to-state transition probabilities on the initial rotational state j of the HF diatom. Specifically, as j increases the background reaction probability increases and moves to higher energies. We also note that the resonances at low energies are mainly due to the contribution from the low-j channels, while for higher energy resonances, the contributions are primarily from the high-j channels even though the low-j channels are energetically accessible.

Figure 4a shows the cumulative reaction probability for the Li + HF → H + LiF reaction over the energy range 0.26−0.50 eV, where energy is given relative to the Li + HF asymptote at its classical equilibrium geometry. The threshold for nonquantal passage over the barrier may be identified with the energy at which the background contribution first equals 0.5.[65−67] In Figure 4a we see that this occurs at $E \approx 0.47-0.49$ eV, which is in reasonable agreement with the zero-point inclusive barrier height (0.45 eV) in Figure 1 and Table 1. Figure 4b shows the cumulative reaction probability below the threshold. The reaction probability is almost zero except at several localized resonance energies, and even at resonance energies, the probability of reaction is small (much less than 0.5). As the energy increases above the effective threshold energy, the background reaction probability (which measures direct reaction) rises gradually. The transition probabilities, however, continue to exhibit sharp resonance features (see Figure 4c). The overall trend for both the background and resonance reaction probabilities is an increase with increasing energy.

4.2. Resonance Energies and Total Widths. To characterize the resonance features, we computed the eigenphase sum Δj on a dense grid of energies (E_j, $j = 1-N_E$) surrounding each resonance. The background contribution was expanded as a polynomial function of the total energy

$$\Delta^{b}(E) = \sum_{l=0}^{N} a_l E^l \qquad (17)$$

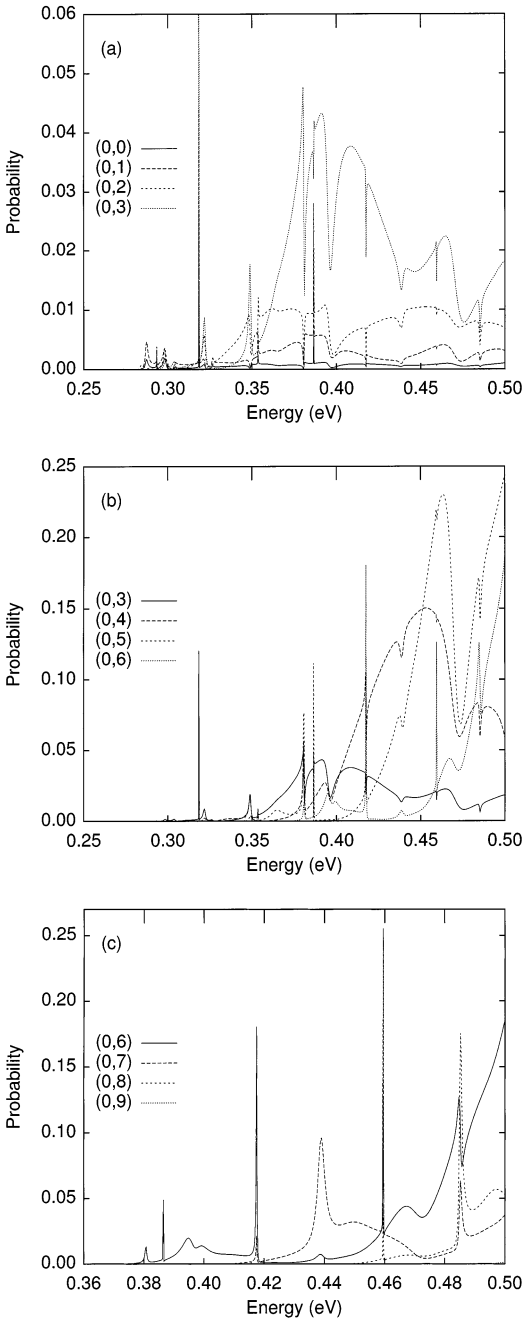

Figure 3. Initial-state-selected reaction probability for the vibrational ground state ($v = 0$) and different rotational states, i.e., the probability of the reaction Li + HF($v = 0, j$) → H + LiF(all v', all j'), as a function of the total energy: (a) $j = 0, 1, 2, 3$, (b) $j = 3, 4, 5, 6$, and (c) $j = 6, 7, 8, 9$.

and eq 12 was fitted to the dense grid of eigenphase sums. To check the stabilization of the fitted E_α and Γ_α, we varied the order N of the polynomial in eq 17 such that

$$\delta^2 = \frac{1}{N^E - N - 2}\sum_{j=1}^{N_E}[\Delta_j - \Delta(E_j)]^2 \qquad (18)$$

was minimized with respect to E_α, Γ_α, and a_l.

Table 3 presents the resonance energy and width for each of the resonances that was observed and characterized. Note that we observe both isolated narrow resonances and broad overlapping resonances. We calculate lifetimes (using eq 8) that range over approximately 3 orders of magnitude from 0.20 to 87 ps.

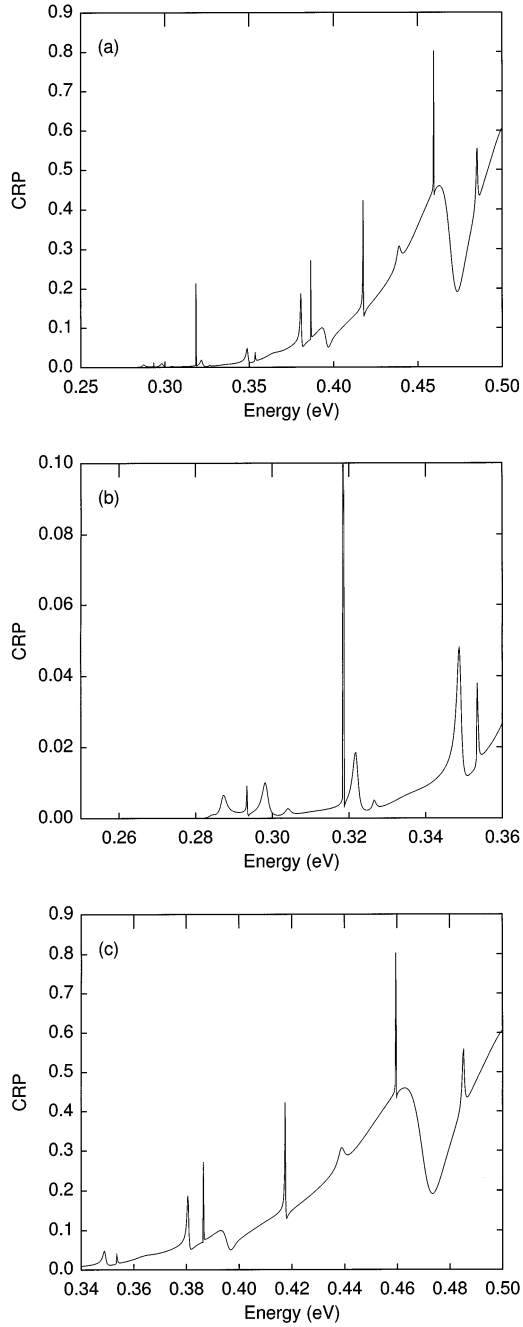

Figure 4. Cumulative reaction probability, i.e., the probability of the reaction Li + HF(all v, all j) → H + LiF(all v', all j'), as a function of the total energy for the energy range (a) 0.25−0.50 eV, (b) 0.25−0.36 eV, and (c) 0.34−0.50 eV.

This is not surprising since the decay rate often depends exponentially on the translational energy associated with the dissociation coordinate.[68−70] Even though not all of the resonances are INRs, the fits to the eigenphase sum are still relatively accurate. The root-mean-square error for each fit is smaller than 0.1%.

Figure 5 illustrates the energy dependence of the eigenphase sum in the region of an isolated narrow resonance with an energy of 0.274 eV, where the dots are the calculated results, the solid line is the fitted curve, and the straight line is the background contribution. As expected,[56−58] there is a rapid increase by π in the eigenphase sum around the resonance.

4.3. Resonance Decay Product State Distributions. For an isolated narrow resonance, the partial widths $\Gamma_{\alpha n}$ (defined in eq 5) may be obtained from any column of the scattering matrix.[59−61] Specifically, the background contribution to each of the scattering matrix elements in eq 4 is expressed as a polynomial of the total energy

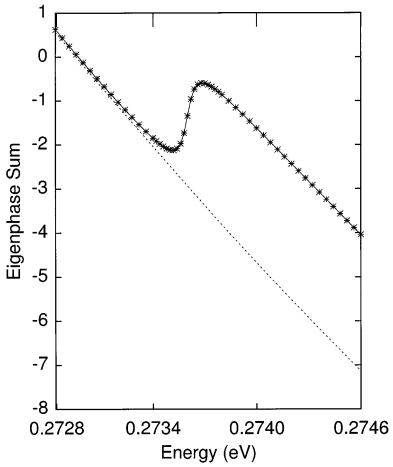

Figure 5. Eigenphase sum as a function of the total energy for the Li + HF → H + LiF reaction at energies near the resonance state energy with $E_\alpha = 0.274$ eV. The asterisks are from the OWVP calculations (smoothed by adding integral multiples of π). The solid line is from the multichannel Breit−Wigner formula. The straight line is the fitted background contribution.

TABLE 3: Energies, Widths, and Lifetimes for Several Observed Resonances

a	E_α (eV)	Γ_α (eV)	τ_α (ps)
1	0.274	7.81×10^{-5}	8.43
2	0.278	1.40×10^{-3}	0.470
3	0.285	2.81×10^{-3}	0.234
4	0.287	1.48×10^{-3}	0.445
5	0.294	1.68×10^{-5}	39.2
6	0.298	1.04×10^{-3}	0.633
7	0.304	7.91×10^{-4}	0.832
8	0.313	3.25×10^{-3}	0.203
9	0.319	7.68×10^{-6}	86.7
10	0.322	6.61×10^{-4}	0.996
11	0.327	9.63×10^{-4}	0.683
12	0.349	5.59×10^{-4}	1.18
13	0.354	2.34×10^{-4}	2.81
14	0.381	6.83×10^{-4}	0.964
15	0.387	1.99×10^{-5}	33.1
16	0.418	2.57×10^{-4}	2.56
17	0.439	3.05×10^{-4}	2.16
18	0.460	5.30×10^{-5}	12.4
19	0.485	3.92×10^{-4}	1.68

$$S_{nn'}^{\mathrm{b}}(E) = \sum_{l=0}^{N} A_{l,nn'} E^l \tag{19}$$

Equation 4 may then be written

$$(E - z_\alpha) S_{nn'}(E) = \sum_{l=0}^{N+1} B_{l,nn'} E^l \tag{20}$$

where

$$B_{0,nn'} = -z_\alpha A_{0,nn'} - \mathrm{i} C_{\alpha nn'} \tag{21}$$

$$B_{l,nn'} = A_{l-1,nn'} - z_\alpha A_{l,nn'} \quad (l = 1, 2, ..., N) \tag{22}$$

$$B_{N+1,nn'} = A_{N,nn'} \tag{23}$$

and

$$C_{\alpha nn'} = \gamma_{\alpha n}\gamma_{\alpha n'} \tag{24}$$

The partial width amplitudes $\gamma_{\alpha n}$ are related to $C_{\alpha nn'}$ by

$$\gamma_{\alpha n'} = \frac{C_{\alpha nn'}}{\sqrt{C_{\alpha nn}}} \tag{25}$$

and $\Gamma_{\alpha n}$ may be calculated using eq 5.

The quantities $\{B_{l,nn'}\}$ may be obtained by fitting eq 20 to the calculated OWVP scattering matrix elements $S_{nn',j}$ and minimizing the quantity

$$\epsilon_n^{\,2} = \sum_{n'=1}^{N_o}\left\{\frac{\sum_{j=1}^{N_E}|S_{nn',j} - S_{nn'}(E_j)|^2}{N_E - N}\right\}^{1/2} \tag{26}$$

where N_o is the number of open channels and N_E is the number of energies included in the fit. From $\{B_{l,nn'}\}$, we can calculate $\{A_{l,nn'}\}$ and $C_{\alpha nn'}$ from eqs 21−23.

We present detailed results for two resonances, namely the $E = 0.294$ and 0.304 eV resonances, which have total reactive decay probabilities (calculated by summing the partial widths associated with reactive channels) of 0.03 and 0.53, respectively. At these energies, LiF is in its ground vibrational state, and the maximum rotational quantum number j that is energetically accessible is 18 and 20, respectively. From the partial widths and eq 10, we computed the probability of decay into each rotational state, and the results are plotted in Figure 6. The rotational state profiles do not differ significantly from the rotational state distributions resulting from direct scattering at nearby nonresonant energies. Considering that these calculated rotational state distributions are very sensitive to the anisotropy of the potential energy surface, comparison of the calculated product state distributions to experiment would be a stringent test of theory, but no experimental result is currently available.

A more detailed study of the trends in the partial widths, although potentially illuminating as to the resonance decay mechanism, is not pursued in the present work.

4.4. Bound and Quasibound States. In addition to their energies and widths, the resonance states of Li···FH identified in sections 4.1 and 4.2 can be approximately characterized by a set of three quantum numbers (when $J = 0$, as is the case throughout this paper). We note that for $J > 0$ a more sophisticated analysis is required than the simple one presented below.[71,72]

For resonances trapped in the reactant van der Waals well, one choice for the quantum numbers is (v, n, $j = l$), where v and j are the quantum numbers respectively describing the vibrational and rotational states of the tightly bound diatom HF, and n and l are quantum numbers describing the stretching motion and angular momentum of Li with respect to the center of mass of HF.[71−73] These quantum numbers are useful for interpreting the dynamics of the resonance when the Li atom is far from HF, i.e., when the interaction energy between Li and HF is small.

Alternatively, one may characterize the resonance states with a set of quantum numbers (ν_r, ν_R, ν_χ), where each quantum number represents the vibrational state of one of the normal modes of the system at its minimum energy geometry. The vibrational quantum numbers are listed in the order of decreasing frequencies, i.e., first the HF vibration mode ν_r, then the nonreactive dissociation mode ν_R, and finally the van der Waals bending mode ν_χ. This set of quantum numbers is useful for describing the dynamics of the resonance when Li is close to HF (i.e., when Li and HF are strongly interacting) and the system is in the deep reactant van der Waals well.

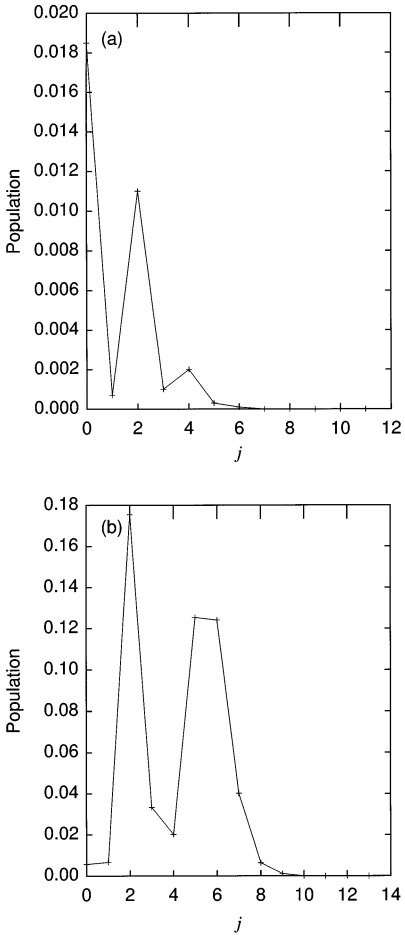

Figure 6. Product rotational state distributions of LiF for the decay of the resonance state with the resonance energy: (a) 0.294 eV; (b) 0.304 eV.

As the system dissociates nonreactively (i.e., to Li + HF) at a resonance energy, the more useful set of quantum numbers changes from the (ν_r, ν_R, ν_χ) set to the (v, n, $j = l$) set, and the two sets of quantum numbers may be correlated in this way. For example, ν_r is approximately equivalent to v, and increased excitation of the bending mode ν_χ is likely to result in increased excitation of j and l. Although both sets of quantum numbers represent idealized situations and are only zero-order approximations, the resonance states are localized over the deep Li···FH van der Waals well, and we expect the (ν_r, ν_R, ν_χ) scheme to be more useful in the present work.

To characterize the quasibound states by the (ν_r, ν_R, ν_χ) scheme for the Li···FH van der Waals complexes, we first computed the bound states of Li···FH. Details of the bound-state calculations are given in section 3.3 and the Appendix. The Li···FH van der Waals well supports 25 bound states, as shown in Table 4. Excitation of the HF vibration requires ∼0.5 eV of energy and therefore all of the bound states have $\nu_r = 0$. The bound states were further characterized by computing the radial wave functions and counting nodes to obtain ν_R. The remaining quantum number ν_χ was assigned as required. Assignment by this method was straightforward, and the energy spacings of the bound states fit regular patterns; i.e., the progression of (0, 0, ν_χ) states is similar to the progression of (0, 1, ν_χ) states, etc. The assignments are shown on the left-hand side of Table 4.

TABLE 4: Bound and Quasibound States of the Li···FH van der Waals Well

bound states			quasibound states		
v_R	v_χ	E_{v_R,v_χ} (eV)	v_R	v_χ	E_{v_R,v_χ} (eV)
0	0	0.062	0	5	0.266
0	1	0.082	2	4	0.279
1	0	0.103	1	5	0.301
0	2	0.112	0	6	0.330
1	1	0.123	2	5	0.334
2	0	0.139	3	5	0.355
1	2	0.148	1	6	0.363
0	3	0.156	2	6	0.389
2	1	0.162	0	7	0.401
3	0	0.170	1	7	0.430
2	2	0.181	2	7	0.450
3	1	0.190	0	8	0.475
4	0	0.197	1	8	0.499
1	3	0.200			
0	4	0.209			
4	1	0.210			
3	2	0.218			
5	0	0.222			
2	3	0.232			
5	1	0.233			
6	0	0.238			
4	2	0.245			
1	4	0.247			
7	0	0.248			
6	1	0.253			

The bound-state energy levels of the Li···FH van der Waals well have been studied previously.[14,17] Reference 17 compares the bound-state energies of potential surfaces obtained from fits to high-level ab initio data calculated at various levels of theory. The most accurate surface that was studied in ref 17 has a zero-point energy of 0.272 eV (relative to the bottom of the well), which agrees well with the value reported in the present work of 0.273 eV. The reported[17] values of the energies of the (0, 0, 1) and (0, 1, 0) states are 0.045 and 0.040 eV relative to the (0, 0, 0) state, respectively. We report values of 0.20 and 0.41 eV for the (0, 0, 1) and (0, 1, 0) states, respectively. Based upon our own bound-state calculations[74] of a previously published surface[14] and the current work, we believe that the (0, 0, 1) state is lower in energy than the (0, 1, 0) state; i.e., the (0, 0, 1) and (0, 1, 0) states in ref 14 (and possibly ref 17) are assigned incorrectly. We do not believe, however, that the surface used in the present work is quantitatively accurate in the van der Waals bend near the van der Waals well; i.e., the energy spacings of the energy levels with varying v_χ quantum numbers are not quantitatively accurate. This defect has been corrected in surface fit **J**,[16] which has energies of 0.34 and 0.48 for the (0, 0, 1) and (0, 1, 0) states, respectively.[74] All of the results in the current paper were obtained using surface fit **H**,[15,16] and the results may therefore not provide quantitative comparison with experiment.

In principle, quasibound states may also be obtained from the energy spectrum obtained by diagonalizing the Hamiltonian in a finite basis. In practice, however, the energies of these states are strongly dependent on the accidental closeness in energy to nearby continuum states. Furthermore, the nodal structure can become obscured as quasibound-state wave functions mix with nearby continuum or quasibound states. By inspection of the radial parts of the unbound wave functions, we were able to definitively determine the energy of and assign quantum numbers for all quasibound states with $v_R = 0$, 1, and 2, as well as one state with $v_R = 3$ in the energy range of the scattering calculations presented in section 4.1. The quasibound states that we identified and assigned are given on the right-hand side of Table 4.

TABLE 5: Li···FH van der Waals Well Bound-State and Quasibound-State Fitted Energy Parameters

parameter	value
ω_R	4.506×10^{-2} eV
ω_χ	1.100×10^{-2} eV
x_R	-2.378×10^{-2}
x_χ	4.539×10^{-3}
$f_{R\chi}$	-5.311×10^{-4} eV
E_0	3.794×10^{-2} eV

To obtain the full spectrum of quasibound states, we fit the bound-state and quasibound-state energies in Table 4 to the same kind of quantum number series[75] as used in conventional spectroscopy, taking the series to second order in the quantum numbers, i.e.

$$E_{\text{fit}}(v_R,v_\chi) = \omega_R\left(v_R+\frac{1}{2}\right) + \omega_\chi\left(v_\chi+\frac{1}{2}\right) + x_R\omega_R\left(v_R+\frac{1}{2}\right)^2 + x_\chi\omega_\chi\left(v_\chi+\frac{1}{2}\right)^2 + f_{R\chi}\left(v_R+\frac{1}{2}\right)\left(v_\chi+\frac{1}{2}\right) + E_0 \quad (27)$$

The root-mean-square (rms) error

$$\Delta \equiv \sqrt{\sum_{v_R,v_\chi} \left(E_{\text{fit}}(v_R,v_\chi) - E_{v_R,v_\chi}\right)^2} \quad (28)$$

was minimized with respect to ω_R, ω_χ, x_R, x_χ, $f_{R\chi}$, and E_0, where E_{v_R,v_χ} are the calculated bound-state and quasibound-state energies in Table 3, and the sum in eq 28 runs over all observed states. The best-fit parameters for eq 27 are given in Table 5, and the resulting fit has a rms error of 0.006 eV. Using the fitted parameters, the full spectrum of quasibound states can be obtained, and the calculated E_{v_R,v_χ} (from Table 4) and fitted $E_{\text{fit}}(v_R,v_\chi)$ quasibound-state energies are given in Table 6 for the energy range in Figures 2−4.

4.5. Characterization of the Observed Resonances and Decay Mechanisms. The quantized energy of the saddle point for reaction is 0.45 eV including zero-point energy in the modes orthogonal to the reaction coordinate,[65] and this energy is within the energy range of total energies considered in the present study (0.26−0.50 eV). It is possible that we may observe a "barrier passage" resonance corresponding to the decrease in the kinetic energy of the system as it passes over the transition state barrier.[58] Barrier passage resonances have short lifetimes (and therefore large widths), and we may associate such a resonance with a broad increase in the cumulative reaction probability between 0.45 and 0.50 eV; we will not analyze this further. The product van der Waals complex LiF···H is not bound when zero-point energy is included as shown in Figure 1. We therefore consider all of the resonances in Table 3 to correspond to trapped-state resonances localized over the reactant van der Waals well.

The resonance energy widths vary over several orders of magnitude (from 8×10^{-6} to 3×10^{-3} eV), and trends in the widths may be explained by assigning (v_r, v_R, v_χ) quantum numbers to the resonances. Assignments were made using the estimated quasibound-state energies in Table 6 as follows: Below the threshold energy (∼0.35 eV) there is a one-to-one correspondence between the scattering resonance energies and the fitted quasibound-state energies for the quasibound states when the $v_R = 0$ and 1 are excluded. We conclude that quasibound states with $v_R = 0$ and 1 have widths too small (smaller than 10^{-6} eV) to observe in the scattering calculations presented here.

TABLE 6: Fitted and Calculated Li···FH Quasibound-State Energies and Assigned Resonance Energies and Widths

v_R	v_χ	$E_{fit}(v_R,v_\chi)$ (eV)	E_{v_R,v_χ} (eV)	E_α (eV)	Γ_α (eV)
4	3	0.278		0.274	7.81×10^{-5}
6	2	0.278		0.278	1.40×10^{-3}
7	2	0.288		0.285	2.81×10^{-3}
1	5	0.294	0.301		
8	2	0.294		0.287	1.48×10^{-3}
5	3	0.298		0.298	1.04×10^{-3}
3	4	0.300		0.294	1.68×10^{-5}
6	3	0.312		0.304	7.91×10^{-4}
0	6	0.321	0.330		
7	3	0.322		0.313	3.25×10^{-3}
4	4	0.323		0.327	9.63×10^{-4}
2	5	0.326	0.334	0.319	7.68×10^{-6}
8	3	0.327		0.322	6.61×10^{-4}
5	4	0.342		0.354	2.34×10^{-4}
3	5	0.354	0.355	0.349	5.59×10^{-4}
6	4	0.356			
1	6	0.358	0.363		
7	4	0.366			
8	4	0.370			
4	5	0.377		0.381	6.83×10^{-4}
2	6	0.390	0.389	0.387	1.99×10^{-5}
5	5	0.396			
0	7	0.396	0.401		
6	5	0.409			
3	6	0.418		0.418	2.57×10^{-4}
7	5	0.418			
8	5	0.422			
1	7	0.432	0.430		
4	6	0.440		0.439	3.05×10^{-4}
5	6	0.458			
2	7	0.464	0.450	0.460	5.30×10^{-5}
6	6	0.471			
0	8	0.479	0.475		
7	6	0.479			
8	6	0.483			
3	7	0.490		0.485	3.92×10^{-4}

Above threshold, the nonresonant reaction probability increases, and the cumulative reaction probability (CRP) energy profile becomes more complicated and contains several broad and overlapping features that are not characterized in Table 3. We assign the observed scattering resonances by again excluding the $v_R = 0$ and 1 quasibound states and based on closeness in energy to the computed quasibound states. There are several missing states, which may be explained as due to the complicated CRP structure above threshold. The missing states have radial dissociation quantum numbers with $v_R \leq 1$ or $v_R \geq 5$. We interpret this finding to indicate that the small-v_R quasibound states have energy widths too small to observe and the high-v_R quasibound states resemble continuum states, have short lifetimes, and have broad, overlapping resonance features that are lost in the nonresonant reactive background probability.

The rms error of the observed and fitted resonance energies is approximately equal to the rms error of the bound-state energies (0.005 eV).

Figure 7 shows the energy width of the scattering resonance as a function of its assigned radial quantum number v_R. There is a strong exponential dependence of the resonance width on the dissociation energy as observed previously.[69] The trend persists over several orders of magnitude in the energy widths, and this strengthens our confidence in the accuracy of the quasibound-state quantum number assignments in Table 6. Although the trends in Table 6 are systematic, some irregularity persists, probably due to the precise but accidental positioning of each resonance energy with respect to asymptotic quantum states.

The scattering resonances undergo the following decay mechanism: At a quasibound-state resonance energy, the system is delayed (i.e., there in an increase in probability density) in the van der Waals well before the transition state barrier, resulting in enhanced tunneling to form the LiF product. The lifetime of the trapped state is determined by the overlap of the quasibound-state radial function with unbound continuum functions of the same translational energy. This overlap depends exponentially on the translational energy and therefore on the radial quantum number.

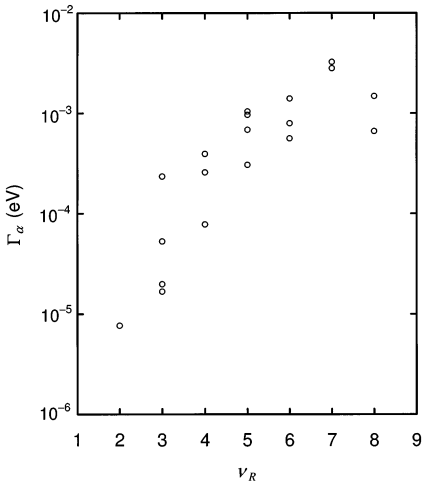

Figure 7. Resonance widths as a function of the translational quantum number. Note that the ordinate scale is logarithmic.

5. Summary

The Li + HF → H + LiF reaction has been investigated in detail using the OWVP full-dimensional time-independent quantum scattering approach to calculate scattering matrix elements, from which we calculated state-to-state, initial-state-specific, and cumulative reaction probabilities. The reaction probabilities are very well converged so that the resonance structure is not lost in the noise, indicating the robustness of the methods being used. All the dynamical features have been recovered, thereby permitting a precise description of resonance states. The scattering resonances were identified in terms of their complex resonance energies.

The Li + HF → H + LiF reaction exhibits a threshold near 0.35 eV, and below the threshold energy the reaction takes place via a mechanism of resonance tunneling, which results in several resonance spikes in the cumulative reaction probability. When the energy is above the threshold, the reaction is governed by both direct and resonance mechanisms. The resonance complexes populated by the collisions can decay nonreactively either by resonance tunneling through the centrifugal barrier in the entrance valley or by energy transfer from the bending mode to the nonreactive dissociation mode. The sum of the reactive and nonreactive rates of decay have been calculated from the fitted resonance widths, with lifetimes ranging from 0.20 to 87 ps.

For two resonances, the product LiF rotational state distributions that result from decay of the resonance complex have been calculated.

We have determined the resonance state energies by both scattering and bound-state calculations, and quasibound-state vibrational quantum numbers have been assigned. Below threshold there is excellent agreement between the resonance and quasibound-state energies. Resonances corresponding to quasibound states with $v_R < 2$ are not observed in the scattering

calculations. Above threshold, several resonances are observed that correspond to quasibound states with $2 \leq \nu_R \leq 4$. In both regimes, there is good exponential correlation between the energy width of the resonance and the radial quantum number ν_R.

The present study is particularly intriguing in the context of identifying intrinsically quantum mechanical behavior in chemical reactions. Resonances that lead to sharp quantum mechanical spikes in the reaction probability at energies beneath the classical threshold are one of the most dramatic quantum effects that one can postulate.[45,66,76] The observation of long sequences of such resonances, both in the O + HCl reaction[45] and in the present study of Li + HF, provides a serious reminder of the necessity of checking classical models against quantum mechanical reality when interpreting chemical reactivity, especially subthreshold energies.

In general, bimolecular chemical reactions feature van der Waals attractions on both sides of the transition state barrier, and these wells are often deep enough to support bound states. The dramatically enhanced reactivity (i.e., the resonance in the reaction profile), at energies associated with van der Waals quasibound states, that results from the localization of the wave function at the base of the barrier depends on several factors including the depth and shape of the well, the height and width of the barrier, the mass of the tunneling particles, etc. Recent experimental work on van der Waals complexes has included several examples of radical−molecule systems,[77−80] and it is not clear which of these might potentially show such behavior. The possibility of state-selected coherent reactivity at isolated narrow resonances raises new possibilities for exploiting quantum mechanical phenomena for control and technological advantage.

Acknowledgment. We are pleased to contribute this paper to the Don Kouri Festschrift. His contributions to the quantum theory of chemical reactivity have been essential to modern progress. We thank Yuri Volobuev and Mike Hack for helpful discussions. This work was supported by the National Science Foundation, through Grant CHE-0092019.

Appendix: Bound-State and Quasibound-State Calculations

The basis functions defined by eq 14 and the matrix element evaluation strategies used to obtain the Hamiltonian matrix elements defined by eq 15 have been presented in detail previously in the context of scattering calculations.[43] The application of these strategies to bound-state calculations (as implemented in the computer code ABCSPECTRA[63]) is straightforward. In this appendix, we briefly present some of the details of the bound-state calculations.

We restrict our attention to the case of zero total angular momentum ($J = 0$), and therefore $l = j$, in which case the elements of the overlap matrix in eq 16 can be written

$$S_{\beta'\beta} = \delta_{\upsilon'\upsilon}\delta_{j'j}\int t_{m'}(R)\, t_m(R)\, \mathrm{d}R \tag{A1}$$

where throughout this appendix $\beta = (\upsilon, j, l, m)$ and $\beta' = (\upsilon', j', l', m')$. The translational basis functions t_m are distributed Gaussian functions with evenly spaced centers (R_m^{T}, where $m = 1, ..., n_{\mathrm{trans}}$). The width parameter of the translational basis functions is determined by setting the overlap parameter c of Hamilton and Light.[81]

The Hamiltonian operator in eq 15 can be written

$$H(\mathbf{R},\mathbf{r}) = -\frac{\hbar^2}{2\mu}\frac{1}{R}\frac{\partial^2}{\partial R^2}R + U^{\mathrm{eff}}(\mathbf{R},\mathbf{r}) + \hat{\tau}(\mathbf{r}) \tag{A2}$$

where

$$\mu = \left(\frac{m_{\mathrm{Li}}m_{\mathrm{H}}m_{\mathrm{F}}}{m_{\mathrm{Li}} + m_{\mathrm{H}} + m_{\mathrm{F}}}\right)^{1/2} \tag{A3}$$

$$U^{\mathrm{eff}}(\mathbf{R},\mathbf{r}) = \frac{\hbar^2}{2\mu}\frac{\hat{l}^2}{R^2} + V^{\mathrm{int}}(\mathbf{R},\mathbf{r}) \tag{A4}$$

$$\hat{\tau}(\mathbf{r}) = -\frac{\hbar^2}{2\mu}\frac{1}{r}\frac{\partial^2}{\partial r^2}r + \frac{\hbar^2}{2\mu}\frac{\hat{j}^2}{r^2} + V^{\mathrm{diat}}(r) \tag{A5}$$

$$V(\mathbf{R},\mathbf{r}) = V^{\mathrm{int}}(\mathbf{R},\mathbf{r}) + V^{\mathrm{diat}}(r) \tag{A6}$$

$$V^{\mathrm{diat}}(r) = \lim_{R\to\infty} V(\mathbf{R},\mathbf{r}) \tag{A7}$$

m_{A} is the mass of atom A, $\hat{l}$ is the orbital (Li to center of mass of HF) angular momentum operator, and $\hat{j}$ is the internal (for the HF diatom) angular momentum operator.

The matrix elements of the first term in eq A2 can be written

$$\left\langle \beta' \middle| -\frac{\hbar^2}{2\mu}\frac{1}{R}\frac{\partial^2}{\partial R^2}R \middle| \beta \right\rangle = -\frac{\hbar^2}{2\mu}\,\delta_{\upsilon'\upsilon}\delta_{j'j}\int t_{m'}(R)\,\frac{\partial^2}{\partial R^2}t_m(R)\,\mathrm{d}R \tag{A8}$$

and can be evaluated analytically. The matrix elements of the second term in eq A2 are

$$\langle\beta'|U^{\mathrm{eff}}(\mathbf{R},\mathbf{r})|\beta\rangle = \int_{R_{\min}}^{R_{\max}} t_{m'}(R)\left[\frac{\hbar^2}{2\mu}\frac{l(l+1)}{R^2}\delta_{\upsilon'\upsilon}\delta_{l'l} + V_{n'n}{}^{\mathrm{int}}(R)\right]t_m(R)\,\mathrm{d}R \tag{A9}$$

where $n = (\upsilon, j, l)$, $n' = (\upsilon', j', l')$

$$V_{n'n}{}^{\mathrm{int}}(R) = \int \phi_{\upsilon'j'}(r)\, y_{j'l'}(\hat{\mathbf{R}},\hat{\mathbf{r}})\, V^{\mathrm{int}}(\mathbf{R},\mathbf{r})\, \phi_{\upsilon j}(r)\, y_{jl}(\hat{\mathbf{R}},\hat{\mathbf{r}})\,\mathrm{d}\hat{\boldsymbol{R}}\,\mathrm{d}\mathbf{r} = \sum_{i=1}^{N_{\mathrm{QV}}} w_{n'n}{}^{i}\sum_{\lambda=0}^{\lambda_{\max}} \upsilon_{\lambda}{}^{\mathrm{int}}(R,r_i) f_{n'n}{}^{\lambda} \tag{A10}$$

$$\upsilon_{\lambda}{}^{\mathrm{int}}(R,r) = \frac{2\lambda+1}{2}\int d(\cos\gamma)\, P_{\lambda}(\cos\gamma)\, V^{\mathrm{int}}(R,r,\cos\gamma) \tag{A11}$$

$$\cos\gamma = \hat{\mathbf{R}}\cdot\hat{\mathbf{r}} \tag{A12}$$

$P_\lambda(\cos\gamma)$ are the Legendre polynomials, and $f_{n'n}{}^{\lambda}$ are the $J = 0$ Percival−Seaton coefficients.[82,83] The radial integral in eq A9 is handled by N_{rep} repetitions of N_{GL}-point Gauss−Legendre quadrature. Optimized vibrational quadrature with the Gauss ground-state option[84] is used to obtain the weights $w_{nn'}{}^{i}$ and nodes r_i in eq A10. The angular integral in eq A11 is carried out using N_{QA}-point Gauss−Legendre quadrature. Matrix elements of the third term in eq A2 may be simplified because the functions $\phi_{\upsilon j}$ are eigenfunctions of $\hat{\tau}$, i.e.

$$\langle\beta'|\hat{\tau}|\beta\rangle = S_{\beta'\beta}\epsilon_{\upsilon j} \tag{A13}$$

where $\epsilon_{\upsilon j}$ is the diatomic energy of the state $\phi_{\upsilon j}$.

The HF diatomic problem is solved in a harmonic oscillator basis $|h\rangle$, where $h = 0, ..., N_{\mathrm{HO}} - 1$. The resulting

TABLE 7: LiFH Bound-State and Quasibound-State Basis Set and Numerical Parameters

parameter[a]	set 1	set 2
N_{HO}	20	25
N_{QV}	20	25
N_{QA}	50	60
N_{rep}	40	55
N_{GL}	7	7
S_{min} (a_0)	0.5	0.2
S_{max} (a_0)	12	14
E_{asym} (eV)	2.8	3.0
S_1^T (a_0)	2.73	2.23
$S_{n_{trans}}^T$ (a_0)	9.77	10.33
Δ (a_0)	0.11	0.10
c	0.9	0.8
n_{asym}	132	161
n_{trans}	64	81
n_{bas}	8448	13041

[a] See the Appendix for definitions of the parameters.

matrix elements are evaluated by writing

$$\langle h'|H^j_{diat}|h\rangle = \delta_{h'h}\hbar\omega\left(h+\frac{1}{2}\right) + \left\langle h'\left|\frac{\hbar^2}{2\mu}\frac{j(j+1)}{r^2} + V_{diat}(r) - V_{HO}(r)\right|h\right\rangle \quad \text{(A14)}$$

and using (N_{HO} + 14)-point Gauss−Hermite quadrature. The harmonic frequency ω is obtained from the second derivative of the HF asymptotic potential at its minimum-energy bond distance. This frequency is also used to determine the exponential parameter of the HO basis functions and the harmonic potential term V_{HO}. The resulting matrices (there is one matrix for each value of j) are diagonalized to obtain the required eigenenergies ϵ_{vj} and eigenfunctions ϕ_{vj}. All asymptotic eigenfunctions ϕ_{vj} with energies ϵ_{vj} less than E_{asym} (relative to the bottom of the asymptotic HF potential curve) are included as basis functions, where E_{asym} is a parameter with respect to which the results are converged. The number of such asymptotic basis functions is n_{asym}.

Once the matrix elements for the Hamiltonian and overlap matrices were calculated, version 2.0 of the LAPACK linear algebra package[85] was used to solve the generalized eigenvalue equation

$$\underline{\underline{H}}\underline{c} = \underline{\underline{E}}\,\underline{\underline{S}}\underline{c} \quad \text{(A15)}$$

where the underline and the double underline indicate vectors and matrices in the vibrational state space, respectively.

Two sets of numerical and basis set parameters are given in Table 7. The mass-scaled parameters R_{min} and R_{max} (of eq A9) and R_m^T are related to the distances S_{min}, S_{max}, and S_m^T by

$$S_{min} = R_{min}/M \quad \text{(A16)}$$

$$S_{max} = R_{max}/M \quad \text{(A17)}$$

$$S_m{}^T = R_m^T/M \quad \text{(A18a)}$$

$$= S_1^T + (m-1)\Delta \quad \text{(A18b)}$$

where

$$M = \left(\frac{m_{Li}(m_H+m_F)^2}{m_H m_F(m_{Li}+m_H+m_F)}\right)^{1/4} \quad \text{(A19)}$$

The total number of basis functions is $n_{bas} = n_{asym}n_{trans}$. The energies of the bound states computed using the two basis sets differ by less than 0.1%.

References and Notes

(1) Zeiri, Y.; Shapiro, M. *Chem. Phys.* **1978**, *31*, 217.
(2) Chen, M. M. L.; Schaefer, H. F., III *J. Chem. Phys.* **1980**, *72*, 4376.
(3) Carter, S.; Murrell, J. N. *Mol. Phys.* **1980**, *41*, 567.
(4) Laganà, A.; Garcia, E. *Theochem* **1984**, *16*, 91.
(5) Garcia, E.; Laganà, A. *Mol. Phys.* **1984**, *52*, 1115.
(6) Paniagua, M.; Aguado, A. *Chem. Phys.* **1989**, *134*, 287.
(7) Palmeiri, P.; Laganà, A. *J. Chem. Phys.* **1989**, *91*, 7303.
(8) Suarez, C.; Aguado, A.; Tablero, C.; Paniagua, M. *Int. J. Quantum Chem.* **1994**, *52*, 935.
(9) Aguado, A.; Suarez, C.; Paniagua, M. *Chem. Phys.* **1995**, *201*, 107.
(10) Aguado, A.; Paniagua, M.; Lara, M.; Roncero, O. *J. Chem. Phys.* **1997**, *106*, 1013.
(11) Aguado, A.; Paniagua, M.; Lara, M.; Roncero, O. *J. Chem. Phys.* **1997**, *107*, 10085.
(12) Laganà, A.; Gervasi, O. Garcia, E. *Chem. Phys. Lett.* **1998**, *143*, 174.
(13) Laganà, A.; d. Aspuru, G. O.; Garcia, E. *J. Chem. Phys.* **1998**, *168*, 3886.
(14) Burcl, R.; Piecuch, P.; Špirko, V.; Bludský, O. *Int. J. Quantum Chem.* **2000**, *80*, 916.
(15) Jasper, A. W.; Hack, M. D.; Chakraborty, A.; Truhlar, D. G.; Piecuch, P. *J. Chem. Phys.* **2001**, *115*, 7945.
(16) Jasper, A. W.; Hack, M. D.; Truhlar, D. G.; Piecuch, P. *J. Chem. Phys.* **2002**, *116*, 8353.
(17) Burcl, R.; Piecuch, P.; Špirko, V.; Bludský, O. *Theochem* **2002**, *591*, 151.
(18) Becker, C. H.; Casavecchia, P.; Tiedermann, P. W.; Valentini, J. J.; Lee, Y. T. *J. Chem. Phys.* **1980**, *73*, 2833.
(19) Parker, G. A.; Pack, R. T; Laganà, A. *Chem. Phys. Lett.* **1993**, *202*, 75.
(20) Baer, M.; Last, I.; Loesch, H.-J. *J. Chem. Phys.* **1994**, *101*, 9648.
(21) Parker, G. A.; Laganà, A.; Crocchianti, S.; Pack, R. T *J. Chem. Phys.* **1995**, *102*, 1238.
(22) Gogtas, F.; Balint-Kurti, G. G.; Offer, A. R. *J. Chem. Phys.* **1996**, *104*, 7927.
(23) Zhu, W.; Wang, D.; Zhang, J. Z. H. *Theor. Chem. Acc.* **1997**, *96*, 31.
(24) Lara, M.; Aguado, A.; Roncero, O.; Paniagua, M. *J. Chem. Phys.* **1998**, *109*, 9391.
(25) Althorpe, S. C.; Kouri, D. J.; Hoffman, D. K. *J. Phys. Chem. A* **1998**, *102*, 9494.
(26) Aoiz, F. J.; Martinez, M. T.; Menéndez, M.; Sáez Rábanos, V.; Verdasco, E. *Chem. Phys. Lett.* **1999**, *299*, 25.
(27) Laganà, A.; Bolloni, A.; Crocchianti, S.; Parker, G. A. *Chem. Phys. Lett.* **2000**, *324*, 466.
(28) Lara, M.; Aguado, A.; Paniagua, M.; Roncero, O. *J. Chem. Phys.* **2000**, *113*, 1781.
(29) Aoiz, F. J.; Verdasco, E.; Sáez Rábanos, V.; Loesch, H. T., Menéndez, M.; Stienkemeier, F. *Phys. Chem. Chem. Phys.* **2000**, *2*, 541.
(30) Aoiz, F. J.; Martinez, M. T.; Sáez Rábanos, V. *J. Chem. Phys.* **2001**, *114*, 8880.
(31) Laganà, A.; Crocchianti, S. *J. Phys. Chem. A* **2001**, *105*, 2361.
(32) Laganà, A.; Bolloni, A.; Crocchianti, S. *Phys. Chem. Chem. Phys.* **2002**, *2*, 535.
(33) Alvarino, J. M.; Aquilanti, V.; Cavalli, S.; Crocchianti, S.; Laganà, A.; Martinez, M. T. *J. Chem. Phys.* **1997**, *107*, 3339.
(34) Alvarino, J. M.; Aquilanti, V.; Cavalli, S.; Crocchianti, S.; Laganà, A.; Martinez, M. T. *J. Phys. Chem. A* **1998**, *102*, 9638.
(35) Stereochemistry and Control in Molecular Reaction Dynamics. *Faraday Discuss.* **1999**, *113*.
(36) Paniagua, M.; Aguado, A.; Lara, M.; Roncero, O. *J. Chem. Phys.* **1998**, *109*, 2971.
(37) Paniagua, M.; Aguado, A.; Lara, M.; Roncero, O. *J. Chem. Phys.* **1999**, *111*, 6712.
(38) Hudson, A. J.; Oh, H. B.; Polanyi, J. C.; Piecuch, P. *J. Chem. Phys.* **2000**, *113*, 9897.
(39) Aguado, A.; Lara, M.; Paniagua, M.; Roncero, O. *J. Chem. Phys.* **2001**, *114*, 3440.
(40) Sun, Y.; Kouri, D. J.; Truhlar, D. G.; Schwenke, D. W. *Phys. Rev. A* **1990**, *41*, 4857.
(41) Schwenke, D. W.; Mielke, S. L.; Truhlar, D. G. *Theor. Chim. Acta* **1991**, *79*, 241.
(42) Tawa, G. J.; Mielke, S. L.; Truhlar, D. G.; Schwenke, D. W. *J. Chem. Phys.* **1994**, *100*, 5751.
(43) Tawa, G. J.; Mielke, S. L.; Truhlar, D. G.; Schwenke, D. W. In *Advances in Molecular Vibrations and Collision Dynamics: Quantum*

Reactive Scattering; Bowman, J. M., Ed.; JAI: Greenwich, CT, 1994; Vol. 2B, pp 45−116.
(44) Zou, S.; Skokov, S.; Bowman, J. M. *Chem. Phys. Lett.* **2001**, *339*, 290.
(45) Xie, T.; Wang, D.; Bowman, J. M.; Manolopoulos, D. E. *J. Chem. Phys.* **2002**, *116*, 7461.
(46) Takayanagi, T.; Kurosaki, Y. *Chem. Phys. Lett.* **1998**, *286*, 35.
(47) Takayanagi, T.; Kurosaki, Y. *J. Chem. Phys.* **1998**, *109*, 8929.
(48) Takayanagi, T.; Kurosaki, Y. *Phys. Chem. Chem. Phys.* **1999**, *1*, 1099.
(49) Garrett, B. C.; Truhlar, D. G. *J. Phys. Chem.* **1979**, *83*, 1079.
(50) Isaacson, A. D.; Truhlar, D. G. *J. Chem. Phys.* **1982**, *76*, 1380.
(51) Corchado, J. C.; Chuang, Y.-Y.; Fast, P. L.; Villá, J.; Hu, W.-P.; Liu, Y.-P.; Lynch, G. C.; Nguyen, K. A.; Jackels, C. F.; Gu, M. Z.; Rossi, I.; Coitiño, E. L.; Clayton, S.; Melissas, V. S.; Steckler, R.; Garrett, B. C.; Isaacson, A. D.; Truhlar, D. G. *POLYRATE*, version 8.5.1; University of Minnesota: Minneapolis, 2000.
(52) Newton, R. G. *Scattering Theory of Waves and Particles*, 2nd ed.; Springer-Verlag: New York, 1982.
(53) Kouri, D. J.; Sun, Y.; Mowrey, R. C.; Zhang, J. Z. H.; Truhlar, D. G.; Huag, K.; Schwenke, D. W. In *Mathematical Frontiers in Computational Chemical Physics*; Truhlar, D. G., Ed.; Springer-Verlag: New York, 1988; p 207.
(54) Schwenke, D. W.; Haug, K.; Zhao, M.; Truhlar, D. G.; Sun, Y.; Zhang, J. Z. H.; Kouri, D. J. *J. Phys. Chem.* **1988**, *92*, 3202.
(55) Taylor, J. R. *Scattering Theory*; Wiley: New York, 1972; pp 238−244.
(56) Nesbet, R. K. *Adv. At. Mol. Phys.* **1997**, *13*, 315.
(57) Hazi, A. U. *Phys. Rev. A* **1979**, *19*, 920.
(58) Friedman, R. S.; Truhlar, D. G. In *Multiparticle Quantum Scattering with Applications to Nuclear, Atomic, and Molecular Physics*; Truhlar, D. G., Simon, B., Eds.; Springer-Verlag: New York, 1997; pp 243−281.
(59) Schwenke, D. W.; Truhlar, D. G. *J. Chem. Phys.* **1987**, *87*, 1095.
(60) Mielke, S. L.; Tawa, G. J.; Truhlar, D. G. *Int. J. Quantum Chem.: Quantum Chem. Symp.* **1993**, *27*, 621.
(61) Hack, M. D.; Jasper, A. W.; Volobuev, Y. L.; Truhlar, D. G. *J. Phys. Chem. A* **1999**, *103*, 6309.
(62) Reid, S. A.; Reisler, H. *Annu. Rev. Phys. Chem.* **1996**, *47*, 495.
(63) Jasper, A. W.; Schwenke, D. W.; Truhlar, D. G. *ABCSPECTRA*, version 1.0; University of Minnesota: Minneapolis, 2003.
(64) Schwenke, D. W.; Volobuev, Y. L.; Mielke, S. L.; Tawa, G. J.; Chatfield, D. C.; Sun, Y.; Haug, K.; Allison, T. C.; Friedman, R. S.; Zhao, M.; Halvick, P.; Hack, M. D.; Truhlar, D. G. *VP*, version 18.8; University of Minnesota: Minneapolis, 1999.
(65) Garrett, B. C.; Truhlar, D. G.; Grev, R. S.; Magnuson, A. W. *J. Phys. Chem.* **1980**, *84*, 1730.
(66) Garrett, B. C.; Truhlar, D. G.; Grev, R. S.; Schatz, G. C.; Walker, R. B. *J. Phys. Chem.* **1981**, *85*, 3806.
(67) Chatfield, D. C.; Friedman, R. S.; Truhlar, D. G.; Garrett, B. C.; Schwenke, D. W. *J. Am. Chem. Soc.* **1991**, *113*, 486.
(68) Beswick, J. A.; Jortner, J. *Chem. Phys. Lett.* **1977**, *49*, 13.
(69) Ewing, G. E. *J. Chem. Phys.* **1979**, *71*, 3143.
(70) Ewing, G. E. *Faraday Discuss. Chem. Soc.* **1982**, *73*, 325.
(71) Bratož, S.; Martin, M. L. *J. Chem. Phys.* **1965**, *42*, 1051.
(72) Hutson, J. M. *Adv. Mol. Vib. Collision Dyn.* **1991**, *1A*, 1.
(73) Hutson, J. M. *J. Chem. Phys.* **1988**, *89*, 4550.
(74) Jasper, A. W.; Truhlar, D. G. Unpublished results, 2003.
(75) Herzberg, G. *Molecular Spectra and Molecular Structure. II. Infrared and Raman Spectra of Polyatomic Molecules*; D. Van Nostrand: Princeton, 1945.
(76) Child, M. S. *Mol. Phys.* **1967**, *12*, 401.
(77) Chen, Y.; Heaven, M. C. *J. Chem. Phys.* **1998**, *109*, 5171.
(78) Chen, Y.; Heaven, M. C. *J. Chem. Phys.* **2000**, *112*, 7416.
(79) Lester, M. I.; Pond, B. V.; Marshall, M. D.; Anderson, D. T.; Harding, L. B.; Wagner, A. F. *Faraday Discuss.* **2001**, *118*, 373.
(80) Pond, B. V.; Lester, M. I. *J. Chem. Phys.* **2003**, *118*, 2223.
(81) Hamilton, I. P.; Light, J. C. *J. Chem. Phys.* **1985**, *84*, 306.
(82) Percival, I. C.; Seaton, M. J. *Proc. Cambridge Philos. Soc.* **1957**, *53*, 654,
(83) Arthurs, A. M.; Dalgarno, A. *Proc. R. Soc. London, A* **1960**, *256*, 540.
(84) Schwenke, D. W.; Truhlar, D. G. *Comput. Phys. Commun.* **1984**, *34*, 57.
(85) Anderson, E.; Bai, Z.; Bishof, C.; Blackford, S.; Demmel, J.; Dongarra, J.; Du Croz, J.; Greenbaum, A.; Hammerling, S.; McKenney, A.; Sorensen, D. *LAPACK Users' Guide*; SIAM: Philadelphia, PA, 1999. The LAPACK library of routines may be found at http://www.netlib.org/lapack.